Perturbed-angular-correlation spectroscopy: Structural anomalies in $(Sr,Ca)(Zr_{3.95}Hf_{0.05})P_6O_{24}$ ceramics

Gary L. Catchen, Michael Blaszkiewicz, Lorenz H. Menke, Jr., and Khalid Jamil
Center for Electronic Materials and Devices, and Department of Nuclear Engineering, The Pennsylvania State University, University Park, Pennsylvania 16802

Herbert A. McKinstry, Dinesh K. Agrawal, and Wayne Huebner
Materials Research Laboratory, The Pennsylvania State University, University Park, Pennsylvania 16802
(Received 9 November 1987)

Perturbed-angular-correlation (PAC) spectroscopy measurements were used to characterize the structure of an ionic conducting ceramic $Sr(Zr_{3.95}Hf_{0.05})P_6O_{24}$ (SZP). Hafnium was substituted primarily into the Zr sites to provide the PAC probe nuclei, $^{181}Hf/^{181}Ta$, and the measurements were made over a range of temperatures from 77 to 1320 K. The results of the analysis were compared to the results of a previously reported analysis of measurements on the "isostructural" ceramic, $Ca(Zr_{3.95}Hf_{0.05})P_6O_{24}$ (CZP). The major difference is that the SZP data show two distinct static electric quadrupole interactions that correspond to two distinct, approximately equally numerous Zr sites, whereas the CZP measurements show one well-defined static interaction at approximately 80% of the sites. Another difference is that no time-varying interactions were observed in the SZP measurements—unlike the CZP results which do show them above 960 K. Using the measurements made below 800 K, the SZP sites were characterized in terms of the presence of or the absence of Sr^{2+} ions in the nearest-neighbor environments of the Zr sites. These assignments were based (1) on point-charge-model calculations, which were used to estimate the electric field gradient (EFG) magnitudes at low temperatures, and (2) on the effective Debye-Waller factors, which were determined from the EFG temperature dependence. These factors also were used to estimate a Debye temperature ratio for the sites. Analysis of the measurements made above 800 K did not provide unique PAC parameters. This problem has limited the information content of the high-temperature data.

I. INTRODUCTION

During the last decade, a structural family of ceramics represented by the chemical formula[1] $(M_{II})_6(M_I)_2Zr_4P_6O_{24}$ has received extensive experimental investigation.[2] These ceramics are of technological importance because they exhibit unique properties which are a result of their similar crystal structures, namely: (1) high ionic conductivity, (2) low thermal expansion (but not necessarily similar changes in the a and c lattice parameters), and (3) a wide range of elements that can substitute into the structures. Despite the large number of investigations on these materials, the origins of these properties are not fully understood.

Recently, we have reported the results of a perturbed-angular-correlation (PAC) spectroscopy study of one member of this family, $Ca(Zr_{3.95}Hf_{0.05})P_6O_{24}$ (CZP) (Ref. 3). The PAC technique uses ^{181}Hf radioactive probe atoms (which populate excited states in ^{181}Ta via β^- decay) to measure electric field gradients (EFG) and spin-relaxation effects at the probe nuclei via the nuclear electric quadrupole interaction. In this structure, these probe atoms (ions) substitute into the Zr^{4+} sites. The results of this study indicate: (1) that 80% of the probe sites undergo a well-defined static interaction over most of the temperature range of the measurements (above 77 K and below 966 K), and (2) that time-varying interactions occur at the higher tempertures. These results provide unique information about the transport of and the site occupancy of the Ca^{2+} ions in the CZP structure.

The natural experiment with which to follow the CZP investigation is a study of the strontium analog $Sr(Zr_{3.95}Hf_{0.05})P_6O_{24}$ (SZP). Although these ceramics are structurally similar, they differ markedly in their thermal expansion characteristics and in electrical conductivity. Figure 1 shows the general crystal structure of CZP and SZP which has rhombohedral symmetry. Although a detailed x-ray crystallographic analysis on a similar structure, $Na_{1.11}Zr_2P_{2.89}Si_{0.11}P_{12}$, indicates the space group $R\bar{3}c$,[4,5] the detailed, single-crystal analysis has not been done on either CZP or SZP. But, the powder-pattern analyses of the CZP and SZP structures indicate that the space groups probably are $R\bar{3}$, but they are definitely not $R\bar{3}c$.[6] The thermal expansion of SZP is nonlinear. At temperatures below approximately 800 K, the a- and c-lattice parameters increase slowly with temperture, and above 800 K the c parameter increases rapidly with temperature.[6] But, for CZP, the a parameter decreases and the c parameter increases with temperature which results in a low coefficient of thermal expansion.[2] Similarly, electrical conductivity measurements that we are currently making on these materials show large differences be-

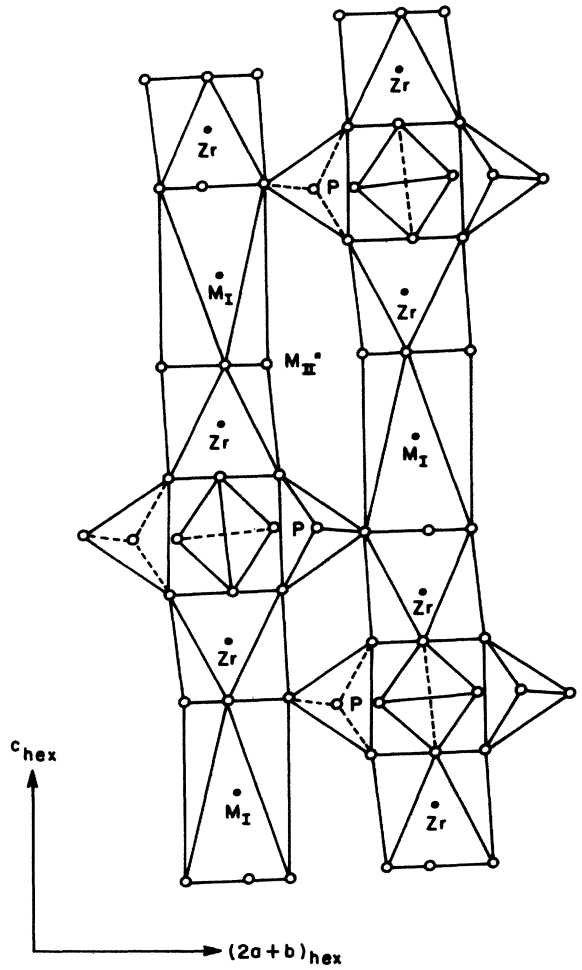

FIG. 1. The basic structure of CZP and SZP. As Ref. 1 describes, the M_I site is the primary site for Ca^{2+} and Sr^{2+} ions in this structure, and the M_{II} site is the secondary site. The relative occupation of these sites is temperature dependent. Also, for divalent cations, at most, half of the M_I sites can be occupied.

tween the CZP and the SZP properties, e.g., in excess of a tenfold difference in the dc conductivities.

PAC spectroscopy is useful for measuring structural nuances that can give rise to differences in properties such as thermal expansion or electrical conductivity. The variations of lattice parameters with temperature are a measure of the anharmonicity of the crystal, and the associated vibrational degrees of freedom affect the temperature dependence of the efg at the Zr site.[3] Therefore, the CZP and SZP structures may show differences in the efg temperature dependences associated with the respective Zr sites. Although the chemistries of Sr^{2+} and Ca^{2+} ions are very similar, the ionic radii, which are 1.04 Å and 1.20 Å, respectively,[5] and the masses differ significantly in magnitude. The differences in ionic radii may cause the site occupancies to be different in the two structures, and the differences in masses may cause time-varying interactions to occur at higher temperatures in the SZP structure than in the CZP structure. In what follows, we report the structural similarities and differences in the context of the derived PAC parameters and the previously developed effective Debye-Waller factors.[3]

II. EXPERIMENTAL DETAILS

The $Sr(Zr_{3.95}Hf_{0.05})P_6O_{24}$ samples were synthesized using the well-known sol-gel technique, which is described in detail elsewhere.[3,7] An x-ray diffraction powder pattern confirmed that the ceramic was a single phase, and no evidence of HfO_2 or ZrO_2 was found. A recent paper[3] gives (1) the relevant radioactive-decay information for $^{181}Hf/^{181}Ta$, (2) the schematic description of the PAC apparatus including the relevant experimental details, and (3) the basic equations describing the PAC theory. Also, because the 615-keV state in ^{181}Ta (which is populated by the β^- decay of ^{181}Hf and decays via the γ-γ cascade) has a relatively long lifetime of 25.7 μsec, no effects of the electronic rearrangement following β^- decay were expected[8] or observed.

Here, we present the specific data analysis procedure. Four correlation functions, $W_{jk}(\theta_{jk},t_i)$, represent the primary experimental data (the subscripts j and k refer to the coincidence between the respective detectors). The experimental perturbation function $A_{22}G_{22}(t_i)$ is obtained by forming the ratio

$$R(t_i)=\frac{2}{3}\left[\left[\frac{W'_{13}(180°,t_i)W'_{24}(180°,t_i)}{W'_{14}(90°,t_i)W'_{23}(90°,t_i)}\right]^{1/2}-1\right] \quad (1)$$

in which the primes indicate that corrections for random coincidences have been made. This ratio (when $A_{44}=0$) is related to the perturbation function by

$$A_{22}G_{22}(t_i)=R(t_i)/\{1+[R(t_i)/2]\} . \quad (2)$$

To obtain the quadrupole frequencies ω_Q and the asymmetry parameters η from the experimental perturbation functions, a two-site model was used to fit the data

$$A_{22}G_{22}(t_i)=A_1\left[S_0+\sum_{k=1}^{3}S_k\exp(-\tfrac{1}{2}\omega_k\delta_1 t_i)\cos(\omega_k t_i)\right]+A_2\left[S_0+\sum_{k=4}^{6}S_k\exp(-\tfrac{1}{2}\omega_k\delta_2 t_i)\cos(\omega_k t_i)\right]+A_3 . \quad (3)$$

A_1 and A_2 are the normalization factors, A_3 is a "background" term, and δ_1 and δ_2 are the line-shape parameters. The frequencies ω_k and the S_k coefficients are taken by analogy to the Abragam-Pound expression[9] which describes a static interaction in a polycrystalline source:

$$G_{22}(t)=S_0+\sum_{k=1}^{3}S_k\cos(\omega_k t) . \quad (4)$$

The parameters in Eq. (3) were determined by nonlinear regression. But, considerable attention was given to evaluating the uniqueness of the derived parameters. We refer to the "free-parameter" fits as fits to Eq. (3) in which only the basic physical constraints were applied, namely, $\omega_1+\omega_2=\omega_3$, $\omega_4+\omega_5=\omega_6$, $\omega_2\geq\omega_1$, $\omega_2\leq 2\omega_1$, $\omega_5\geq\omega_4$, and $\omega_5\leq 2\omega_4$. In addition, we performed "$\eta=0$ constrained" fits in which $\omega_2=2\omega_1$ and $\omega_5=2\omega_4$.

III. RESULTS

Figure 2 presents several of the experimental perturbation functions and the fitted two-site-model functions. To check whether the two-site model was necessary, we applied both the one-site [Eq. (3) with the second term deleted] and the two-site models to one of the 295-K data sets. Figure 3 presents the comparison. In this case, the two-site model provides a much better representation of the data. As a result, the two-site model was applied to all of the data sets. This model produces relatively good fits to the low-temperature data sets, but the model produces less satisfactory fits to the high-temperature data sets. The perturbation functions obtained at several higher temperatures, 730, 820, 910, 970, and 1050 K, appear similar to the 660 K data, and they show increasing degrees of line broadening with increasing temperature.

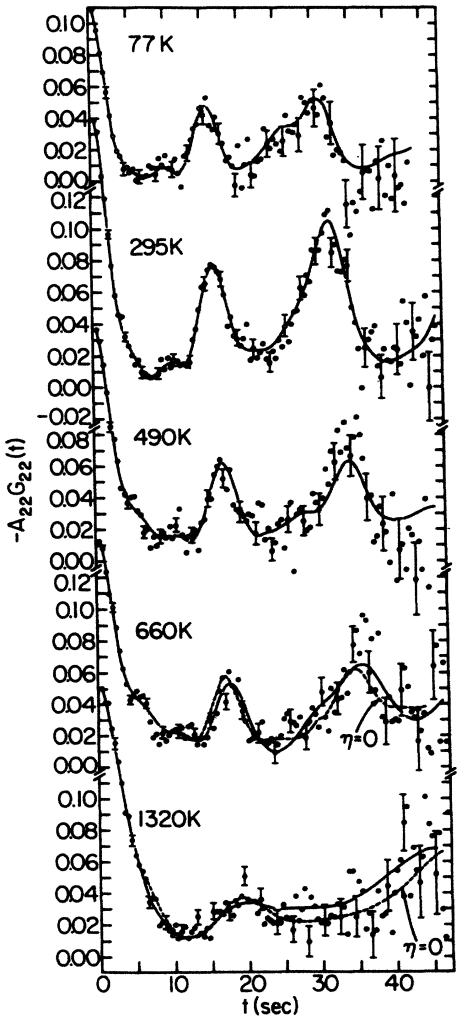

FIG. 2. Several of the perturbation functions for $Sr(Zr_{3.95}Hf_{0.05})P_6O_{24}$ at the indicated temperatures are shown. The solid lines represent free-parameter fits to the two-site model. Where the differences can be shown, the dashed lines represent $\eta=0$ constrained fits. As the temperature increases, the functions broaden. At 1320 K the peaks are barely discernable, but sets of parameters were obtained for the purpose of comparison.

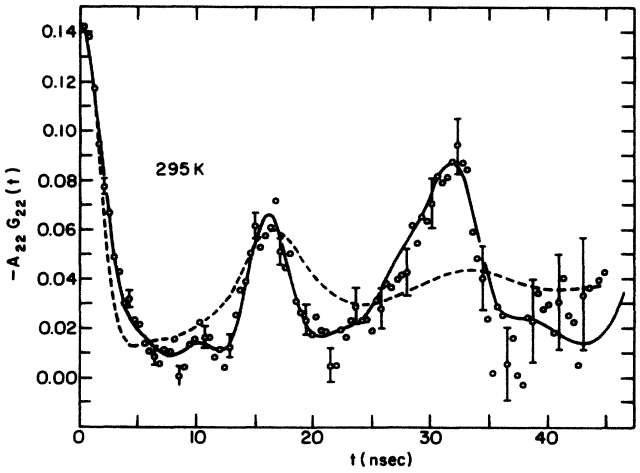

FIG. 3. For one of the 295 K data sets, fits for both the two-site (solid line) and the one-site (dashed line) models are shown.

Figure 4 shows two examples of the high-temperature data. Because the lines are broad and because the second peak occurs at rather long times (in excess of four intermediate-state half lives, i.e., 4×10.8 nsec), the quality of the fits is not as good as in the low-temperature cases. This situation implies that the uniqueness of the derived parameters may be questionable. To address this possibility, we show the free-parameter fits in Fig. 4 from which we derived *large* values of both asymmetry parameters, and we show the $\eta=0$ constrained fits. In these high-temperature examples, the two types of fits do not differ greatly in the shapes of the derived curves and, in the low-temperature data sets, the corresponding differences are insignificant. Although the curves fitted to the high-temperature data sets with $\eta\approx 1$ and with $\eta=0$ appear similar, significant differences do arise in the derived A_i and δ_i parameters, which we discuss below. This apparent ambiguity in the parametric description of the data limits, as well as complicates, the interpretation of the derived interaction frequencies.

For each site i, the quadrupole frequencies ω_{Qi} and the asymmetry parameters η_i were derived from the three respective frequencies ω_i and, for each site, the zz component of the EFG in the principal axis coordinate system V_{zz} (with the Zr site at the origin) was obtained by using the relation $\omega_Q=[(eQV_{zz}/4I(2I-1)\hbar)]$. Figure 5(a) presents the results. Also, the measured values of V_{zz} for CZP are shown for comparison. To characterize these data, we fitted (1) the CZP V_{zz} values, (2) the low-temperature (<800 K) SZP V_{zz} values derived from the free-parameter fits for both the low-frequency interaction

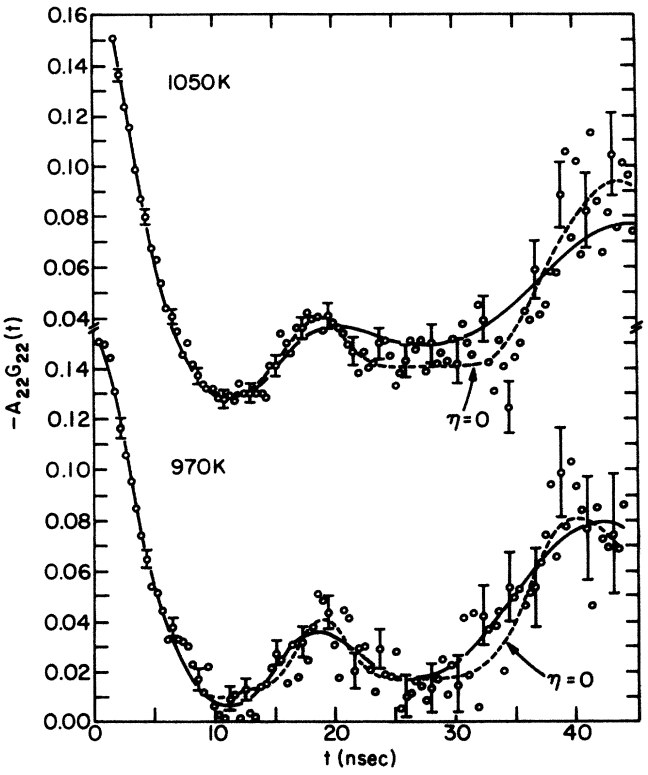

FIG. 4. Two perturbation functions representative of the high-temperature data are shown. Two fits are shown—the solid line is the free-parameter fit and the dashed line is the fit constrained by $\eta_1=0$ and $\eta_2=0$.

and for the high-frequency interaction, and (3) the corresponding values for the $\eta=0$ constrained fits, to the Gaussian expression

$$V_{zz}(T)=V_{zz}(0)\exp(-bT^2)\ . \tag{5}$$

Figure 5(a) also shows the derived b parameters. Reference 3 discusses the physical significance of this expression in detail. Here, we mention that the exponential factor $\exp(-bT^2)$ is an effective Debye-Waller factor, which relates the temperature dependence of the EFG to the vibrational degrees of freedom in the crystal lattice. Figure 5(b) shows the lattice parameters a and c which were measured by high-temperature powder x-ray diffraction.[6]

Figure 6 shows the asymmetry parameters η_1 and η_2 derived from the free-parameter fits for the two respective sites. For the data taken above 800 K, the asymmetry parameters are essentially unity; whereas, with a few exceptions, the parameters for the low-temperature data are close to zero. Corresponding to this large change in the asymmetry parameters, the V_{zz} values for the high-frequency site also appear to change discontinuously. In addition, as Figure 5(b) shows, the c parameter begins to increase more rapidly with temperature at approximately the same range of temperature.

Figures 7(a) and 7(b) present the relative site populations $A_i'=A_i/(A_1+A_2+A_3)$ [as given by Eq. (3)] for the free-parameter fits and for the $\eta=0$ constrained fits, respectively. Except for a spurious result at 295 K, site populations are essentially the same at low temperatures. The background fraction A_3' is insignificant, i.e., less than 10%, throughout the temperature range. However, as the temperature increases, the populations derived from the free-parameter fits show generally that the high-frequency site populates at the expense of the low-frequency site. The data from the $\eta=0$ constrained fit show the opposite result. We have no conclusive criteria to choose one result over the other. But, the structural consideration, namely, that the Zr-site nearest-neighbor environment has axial symmetry, suggests that the $\eta=0$ constrained fits are a more likely representation. Although this choice of fits may provide the most likely set of quadrupole frequencies and asymmetry parameters to represent the high-temperature data, the corresponding relative site populations may not be unique. Therefore, we consider the possibility that the site populations are approximately equal over the entire temperature range and that the apparent site population shift is an artifact. For the five data sets at temperatures greater than 800 K, the average relative populations are $A_1'=0.29$ and $A_2'=0.64$ for the free-parameter fits and $A_1'=0.65$ and $A_2'=0.30$ for the $\eta=0$ constrained fits. But, for these data sets, the free-parameter fits yield approximately

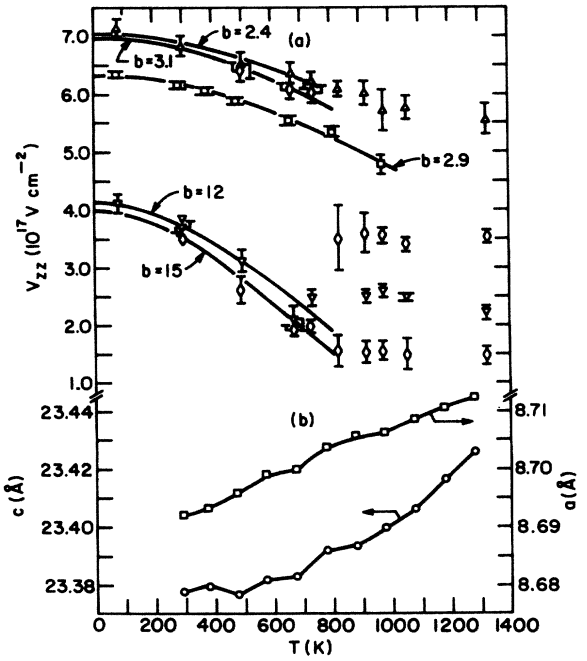

FIG. 5. (a) The temperature dependence of the EFG is shown for: (1) the SZP low-frequency site where the inverted triangles indicate values of V_{zz} derived from the free-parameter fits, and the diamonds indicate the values derived from the $\eta=0$ constrained fits (where the values differ), (2) the SZP high-frequency site where the triangles indicate values from the former fits, and the diamonds indicate values from the latter, and (3) the primary CZP site where the values of V_{zz} are indicated by the squares. To obtain the indicated b parameters (which need to be multiplied by 10^{-7}), the V_{zz} values for $T<800$ K were used. (b) The lattice parameters a and c for SZP are shown. The lines are drawn to guide the eye. Notice that the c parameter begins to increase at approximately 800 K, but the a parameter increases approximately linearly over the temperature range.

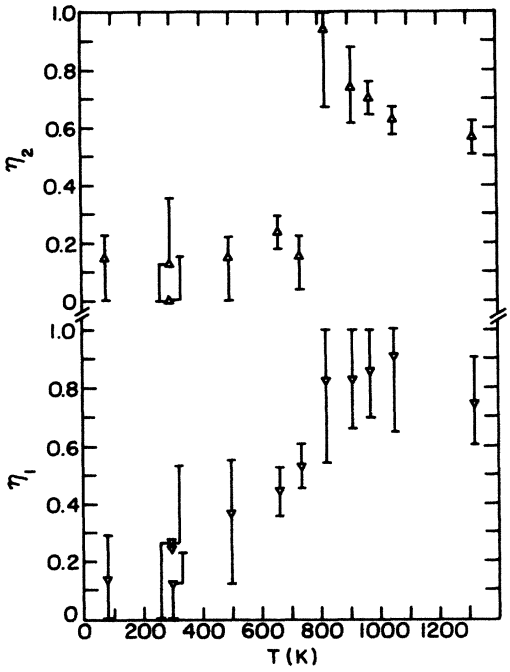

FIG. 6. The derived asymmetry parameters are shown for the free-parameter fits to the SZP data. The inverted triangles refer to the values for the low-frequency site η_1, and the triangles refer to the high-frequency site η_2.

equal values for the frequencies ω_3 and ω_4 but, at low temperatures, these fits give roughly equal values for ω_2 and ω_4. Hence, the shift in relative population values for the free-parameter fits to the high-temperature data sets may be an artifact of the common frequencies. Whereas, in the $\eta=0$ constrained fits, less obvious effects may be

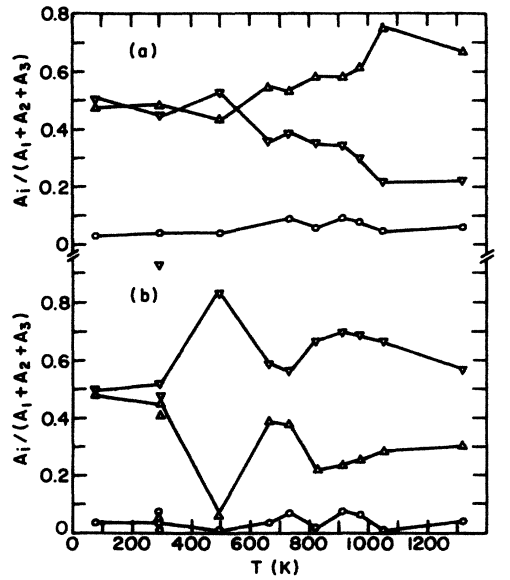

FIG. 7. (a) The relative site populations are shown for the free-parameter fits to the SZP data. The inverted triangles refer to the low-frequency site; the triangles refer to the high-frequency site. The lines are drawn to guide the eye. (b) The relative site populations are shown for the $\eta=0$ constrained fits to the SZP data.

taking place. In either case, the line-shape parameters also may contribute to the apparent differences in the site populations.

Figure 8 shows the line-shape parameters δ_1 and δ_2 for the low- and high-frequency sites, respectively. The line-shape parameters for the low-temperature data are relatively small, i.e., less than 0.2 for most of the fits. Whereas, for the high-temperature data, large fluctuations from data set to data set appear. As Figure 4 indicates, the lines are much broader in the high-temperature data. This fact, in concert with the other pathological feature of the data, namely, the dependence of the relative site population on the frequency constraints, again reflects the problematical nature of obtaining unique parameters for the high-temperature perturbation functions.

IV. DISCUSSION

A. The derived PAC parameters

The salient differences that are most prominent between the SZP and the CZP structures are as follows. The SZP structure has two types of Zr sites that have approximately equal populations at low temperatures, and the extrapolated V_{zz} ($T=0$ K) value for the low-frequency interaction is approximately 60% of the corresponding value for the high-frequency interaction. Whereas, the CZP structure has primarily one well-defined Zr site that has a relative population of approximately 80% over the temperature range considered (77–1180 K).[3] (Note, however, the CZP structure has a small fraction, 20%, of sites that undergo a poorly-defined static interaction at 2–3 times the quadrupole frequency of the major interaction.) The associated value of $V_{zz}(0)$ for the primary interaction in CZP is approximately 12% lower than the corresponding value for the high-frequency site in the SZP structure. But, the derived b

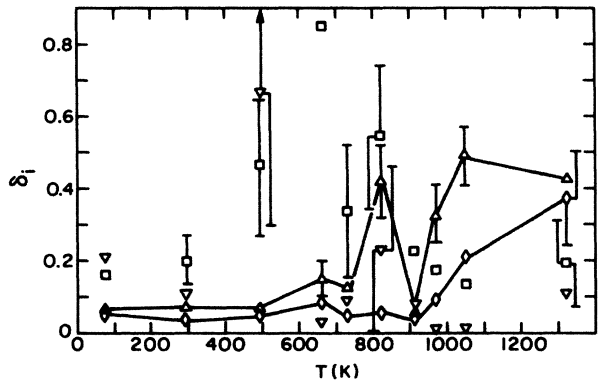

FIG. 8. The line-shape parameters δ_1 and δ_2 are shown for the free-parameter fits where the inverted triangles denote the low-frequency site values, and the triangles denote the high-frequency site values. The line-shape parameters δ_1 and δ_2 are also shown for the $\eta=0$ constrained fits where the squares denote the low-frequency site values, and the diamonds denote the high-frequency site values. The uncertainties are shown for some of the larger δ values and some lines are drawn to guide the eye.

parameters [in Eq. (4)] from the low-temperature data points for SZP bracket the value derived from the CZP data. For the high-frequency interaction in SZP, the V_{zz} and η values derived from the the free-parameter fits show discontinuities in the temperature range near 800 K. Whereas, the V_{zz} values derived from the $\eta=0$ constrained fits decrease continuously with temperature. Additionally, no time-varying interactions in SZP are observed, but, at high temperatures greater than 960 K, a time-varying interaction is observed in CZP.

We consider the EFG's at low temperatures in SZP. The V_{zz} and b-parameter values for the high-frequency interaction in SZP are reasonably close to those for the static interaction in CZP. These two results suggest strongly that the corresponding sites are very similar or identical. Moreover, point-charge-model calculations have been performed for the distorted-octahedral nearest-neighbor environment of the Zr site, in which the point-charge sum includes only six O^{2-}-ion charges.[3] The calculated value of V_{zz} (at 298 K) is within 15% pf the experimental value for CZP and is essentially the same as the SZP value. Now, inclusion of a 2^+ cation charge in the point-charge sum at a distance equal to the Zr-site–$M_{\rm I}$-site distance reduces the magnitude of V_{zz} to approximately 40% of the initial value. (The corresponding experimental value is approximately 60%.) Therefore, the calculated values of V_{zz}—*without* and *with* the 2^+ cation in the sum—agree with the measured values of $V_{zz}(0)$ for the high- and the low-frequency interactions in SZP, respectively (within the accuracy expected from the point-charge model). Given this evidence, we assign the high-frequency interactions to the corresponding sites in SZP and in CZP in which the nearest $M_{\rm I}$ site is vacant. Also, we assign the low-frequency interaction in SZP to a site in which the nearest $M_{\rm I}$ site is occupied by a Sr^{2+} ion. The formula, $(M_{\rm II})_6(M_{\rm I})_2Zr_4P_6O_{24}$, implies that for Ca^{2+} or Sr^{2+} ions at most one-half of the $M_{\rm I}$ sites can be occupied; and when that situation occurs, all of the $M_{\rm II}$ sites are vacant. Therefore, *a priori*, we would expect that both structures would exhibit two static low- and high-frequency interactions corresponding to equally-populated occupied and unoccupied $M_{\rm I}$ sites, respectively. At low temperatures the SZP results agree with this prediction, but the CZP results only show one of the interactions.

We offer the following explanation. Single-crystal x-ray diffraction measurements on the Na analog indicate that the $M_{\rm I}$ sites are occupied in preference to the more numerous, interstitial $M_{\rm II}$ sites.[4] This property may apply to the many members of this family of ceramics,[1] but agreement on this point[10] as well as experimental confirmation is lacking. Moreover, Kohler *et al.*[11] have calculated potential energy surfaces for a similar structure, and their results indicate that the $M_{\rm II}$ site is lower in energy than the $M_{\rm I}$ site. Thus, the energetics as well as sixfold ratio of $M_{\rm II}$ sites to $M_{\rm I}$ sites in these structures favor depopulation of the $M_{\rm I}$ site. Now, during preparation, these CZP and SZP ceramics are sintered at 1570 K. The CZP structure may be such that the potential well corresponding to the $M_{\rm II}$ site is very deep. Then, during sintering, the Ca^{2+} ions would tend to leave the $M_{\rm I}$ site and not return. Alternatively, the SZP structure may have a potential well that is not nearly as deep. And, during sintering, the Sr^{2+} ions may migrate back and forth between $M_{\rm I}$ and $M_{\rm II}$. Although this explanation is not conclusive, the experimental results indicate clearly that cation transport is different in SZP than in CZP.

We comment on two other aspects of the SZP data. Firstly, the discontinuous changes (derived from the free-parameter fits) in V_{zz} at approximately 800 K may result from a phase transition. None of the powder x-ray diffraction data either support or refute this suggestion. Work is in progress to obtain high-temperature x-ray diffraction data on a single crystal. Unfortunately, the analysis of the PAC measurements cannot rule out the possibility of a phase transition. Another interesting observation is that dc conductivity measurements that we have made on SZP do not support a simple activation energy model of Sr^{2+}-ion transport, although support is found in the case of CZP.[3] To elucidate this situation, work is also in progress to obtain ac conductivity measurements on both CZP and SZP. Alternatively, the apparent discontinuous change in V_{zz} and η may, in fact, be a canard. For the high-frequency site, the results of the $\eta=0$ constrained fits show a continuous, slow decrease in the EFG with increasing temperature. This result is analogous to the CZP result. Moreover, because the nearest-neighbor environment of the Zr site is a distorted octahedral environment of O^{2+} ions, we expect the corresponding η values to be close to zero. And, only a massive structure change could cause the η values to increase to unity, i.e., for V_{yy} to vanish.

Secondly, the SZP experimental results show no evidence of time-varying interactions over a range of temperatures up to 1320 K. But, the CZP data show a time-varying interaction at 966 K and at 1180 K.[3] This result may indicate that the sizes of the diffusion pathways for Sr^{2+} ions are different than those for Ca^{2+} ions. Or, alternatively, since the SZP dc conductivity at 1000 K is approximately an order of magnitude lower than the corresponding value for CZP, the Sr^{2+}-ion diffusion rate may be sufficiently low in the SZP structure that nuclear-spin relaxation does not take place at the temperatures of interest.

B. The temperature dependence of the EFG

As we have discussed, there are several vagaries associated with the determination of and the interpretation of the EFG's from the high-temperature data. However, the EFG measurements at low temperatures appear to be reliable. For the SZP low-temperature data, the derived b parameters range from 2.4×10^{-7} K^{-2} to 3.1×10^{-7} K^{-2} for the high-frequency site and 12×10^{-7} K^{-2} to 15×10^{-7} K^{-2} for the low-frequency site. Previously, we have made a correspondence between the factors in Eq. (5) and the expression (in which $eq=V_{zz}$) developed by Nishiyama *et al.*:[3,12]

$$eq(T)=(1-\gamma_{\rm eff})eq^{\rm sc}_{\rm ion}(T)\exp\{-\tfrac{4}{3}k_F^2\langle u^2\rangle(T)\} \qquad (6)$$

in which k_F is the Fermi wave vector and $\langle u^2 \rangle$ is the mean-square displacement. The factors $(1-\gamma_{\text{eff}})eq^{\text{sc}}_{\text{ion}}$ correspond to $V_{zz}(0)$ and the exponential factor corresponds to $\exp(-bT^2)$. After applying the Debye crystal model and making several simplifying assumptions (one of which is that the Debye temperature, Θ, of the crystal is much larger than the crystal temperature), we have obtained

$$\exp(-bT^2)=\exp(-3\hbar^2k_D^2/Mk_B\Theta_D)\times\exp(-2\pi^2\hbar^2k_D^2T^2/Mk_B\Theta_D^3) \quad (7)$$

in which k_D is the Debye wave vector, k_B is the Boltzman constant, and M is the mass of the atoms in the crystal. In this correspondence $b=2\pi^2\hbar^2k_D^2/Mk_B\Theta_D^3$. Although the meanings of either the Debye wave vector k_D or the mass M may not be clear, since Eq. (6) was originally applied to monatomic metal crystals, we only need to assume that these quantities are essentially the same for both Zr sites in SZP. Then, the relationship between derived b parameters for sites 1 and 2 and the associated Debye temperatures is

$$(\Theta_{D1}/\Theta_{D2})=(b_2/b_1)^{1/3} . \quad (8)$$

Using this relationship, we find that $(\Theta_D)_{\text{LF}}=(0.59\pm0.03)(\Theta_D)_{\text{HF}}$, in which the subscripts HF and LF refer to the high-frequency and the low-frequency sites, respectively. Now, the Debye model for monatomic crystals predicts that higher mass crystals have lower Debye temperatures. Above we stated evidence indicating that the nearest-neighbor environment producing the low-frequency interaction may contain a Sr^{2+} ion in the M_{I} site. Whereas, the environment producing the high-frequency interaction may not contain a Sr^{2+} ion in the M_{I} site. This result, namely, that the magnitude of the Debye temperature corresponding to the low-frequency site is approximately 60% of the magnitude of the Debye temperature corresponding to the high-frequency site, is not inconsistent with the site assignments. That is, the additional mass of a Sr^{2+} ion and its associated effect on the vibrational motion near the corresponding Zr site may affect the temperature dependence of the EFG at that site.

V. CONCLUSIONS

In the SZP structure, at low temperatures, two distinct, approximately equally numerous electric quadrupole interactions are observed via the ^{181}Hf/^{181}Ta probe nuclei at the Zr sites. Whereas, in the Ca analog CZP, primarily one well-defined interaction at 80% of the Zr sites is observed. Point-charge-model calculations that are based on x-ray diffraction data suggest that the M_{I} site nearest to the Zr site is vacant during the high-frequency interaction but occupied during the low-frequency interaction. As a result, the SZP structure appears to have some occupied M_{I} sites but the CZP structure does not. This difference could reflect differences in the potential energy surfaces corresponding to the two structures.

The analysis of the high-temperature perturbation functions for SZP does not yield a unique set of parameters. In particular, discontinuities in the EFG's and asymmetry parameters derived from the free-parameter fits imply that a massive structural change occurs above 800 K. But, the high-temperature x-ray powder patterns do not indicate a large change in structure. However, the parameters derived from the $\eta=0$ constrained fits show no discontinuities. Unfortunately, both sets of fits are reasonable representations of the high-temperature data. But, the $\eta=0$ limit is consistent with the low-temperature structure of SZP. That is, the nearest-neighbor O^{2-}-ion configuration with the Zr site and the M_{I}-cation site on the c axis is an axially-symmetric configuration. Additionally, ambiguities in the relative site populations arise as artifacts of the two different types of fits. As a result, the sites at high temperatures cannot be characterized definitively.

For the two Zr sites in the SZP structure, effective Debye-Waller factors were determined from the temperature dependence of the EFG (over the range of low temperatures). The associated Debye temperature for the low-frequency site is approximately 60% of that for the high-frequency site. The effects of the Sr^{2+} ions on vibrational motion near the low-frequency Zr site may be responsible for the specific EFG temperature dependence being different for this site. Similarly, the effects of the Sr^{2+} ions may be responsible for the reduced magnitude of the static EFG corresponding to the low-frequency site. Thus, the PAC measurements have provided information on both dynamic and static effects of the Sr^{2+} ions on the SZP structure. This information indicates subtle differences in the SZP and CZP structures.

ACKNOWLEGMENTS

We thank Professor Morton Kaplan of the Carnegie-Mellon University for much technical guidance and scientific wisdom. We gratefully acknowledge financial support from the Department of Nuclear Engineering and the Fermi Industrial Consortium. We thank Ms. Kathryn Roeder of the Department of Statistics for helping us develop the nonlinear regression program. We thank Mr. Chi-Yuan Huang for making and analyzing the high-temperature x-ray diffraction measurements. We also thank the Pakistan Ministry of Science and Technology and the Pakistan Atomic Energy Commission for giving one of us (K.J.) financial support and a leave of absence, respectively. We acknowledge Dr. Barry E. Scheetz and Dr. L. J. Pilione of the Materials Research Laboratory for much encouragement and technical assistance.

[1]T. Oota and I. Yamai, J. Amer. Ceram. Soc. **69**, 1 (1986).
[2]R. Roy, D. K. Agrawal, J. Alamo, and R. A. Roy, Mater. Res. Bull. **19**, 471 (1984), and the references found therein.
[3]G. L. Catchen, L. H. Menke, Jr., M. Blaszkiewicz, K. Jamil, D. K. Agrawal, W. Huebner, and H. A. McKinstry, Phys. Rev. B **37**, 4839 (1988).
[4]R. M. Hazen, L. W. Finger, D. K. Agrawal, H. A. McKinstry, and A. J. Perrotta, J. Mater. Res. **2**, 329 (1987).
[5]N. G. Chernorukov, I. A. Korshunov, and T. V. Prokof'eva, Sov. Phys. Crystallogr. **23**, 475 (1979).
[6]H. A. McKinstry, Chi-Yuan Huang, and D. K. Agrawal, in Proceedings of the 1987 Fall Meeting of the Materials Research Society in Boston, 1987 (unpublished).
[7]D. K. Agrawal, S. Y. Limaye, R. Roy, and Y. Mehrotra, J. Amer. Ceram. Soc. (to be published).
[8]D. A. Shirley and H. Haas, Ann. Rev. Phys. Chem. **23**, 385 (1972).
[9]A. Abragam and R. Pound, Phys. Rev. **92**, 943 (1953).
[10]H. Y.-P. Hong, Mater. Res. Bull. **11**, 173 (1976).
[11]H. Kohler, H. Schultz, and O. Melnikov, Mater. Res. Bull. **18**, 1143 (1983).
[12]K. Nishiyama, F. Dimmling, Th. Kornrumpf, and D. Riegel, Phys. Rev. Lett. **37**, 357 (1976).